Journal of Environmental Management 392 (2025) 126661

Contents lists available at ScienceDirect

Journal of Environmental Management

journal homepage: www.elsevier.com/locate/jenvman

Research article

Sustainable removal of ammonia via a coupled ion exchange and electrolysis system

Jeong-Hee Kang [a], Gyung-Geun Oh [a], MyungSuk Son [b], Sungwon Kang [a,*]

[a] Department of Environmental Research, Korea Institute of Civil Engineering and Building Technology, 283 Goyang-daero, Insanseo-gu, Goyang, 10223, Republic of Korea

[b] Future Environment Energy Center, Korea Testing Laboratory, 87 Digital-ro, Guro-gu, Seoul, 08389, Republic of Korea

ARTICLE INFO

Keywords:
Ammonia recovery
Anaerobic digestion dewatering liquor
Prussian blue analog
Ion exchange
Electrolysis

ABSTRACT

Anaerobic digestion (AD) sludge dewatering liquor is associated with a persistent problem of the total ammonia nitrogen (TAN) removal. We investigated a coupled system consisting of ion exchange and electrolysis. TAN was recovered using a Prussian blue analog (PBA)-immobilized adsorbent and removed by electrolysis along with hydrogen gas production. Batch tests revealed that PBA exclusively adsorbed TAN and was recovered by ion exchange, despite the application of actual wastewater. Langmuir and Temkin models showed good fits with the experimental data ($R^2 > 0.99$). In continuous column tests, >87.6 % TAN was consistently recovered without a decrease in the adsorption capacity for 12 cycles. TAN recovered in the regenerant was removed within 270 min to <30 mg-N/L, and the oxidation rate lasted without any notable change. Although NO_3^- and K^+ concentrations increased continuously to >1 M, the electro-oxidation rate was stable. Investigation of the PBA surface demonstrated that no accumulation of competing ions occurred, and ion exchange was effectively performed. The capital and operational expenditures were determined as 4.109 and 3.191 M$, respectively. This suggested that the proposed system is comparable to the various TAN removal processes. The proposed system is a promising technology for recovering TAN and producing hydrogen gas.

1. Introduction

Ammonia (NH_3) is a crucial commodity widely used in the production of fertilizers, refrigerants, explosives, textiles, and pesticides. Owing to its enormous global consumption, considerable amounts of energy are required for ammonia synthesis, leading to substantial CO_2 emissions (Wang and Meyer, 2019). The manufacture of ammonia through the Haber–Bosch process has led to the emission of 426 Mt of CO_2 equivalent, accounting for 2 % of total global emissions (Liu et al., 2020). Over the past decade, ammonia has emerged as a leading hydrogen carrier because of its ease of liquefaction, storage, and transportation. Beyond its role as a hydrogen carrier, ammonia can also be directly utilized to generate clean electricity via injection into fuel cells. With its high energy density and carbon-free combustion, ammonia offers a promising pathway for reducing CO_2 emissions and addressing global energy and climate challenges (Vigneswaran et al., 2025; Wan et al., 2021). Given its versatility, the market price of ammonia has increased from 200 U.S. dollars ($)/ton in 2019 to 480 $/ton in 2024 (Im et al., 2025; U.S. Geological Survey, 2024). However, ammonia is also a potent environmental contaminant, affecting air, water, and soil ecosystems. Traditional biological treatment methods, such as nitrification and denitrification, which are widely used to remove ammonia, consume energy comparable to that of the Haber–Bosch process (Dai et al., 2024). These circumstances highlight the potential of ammonia recovery from wastewater as a more sustainable alternative. Recovery not only enables the reuse of a valuable chemical but also supports pollutant removal, contributing to environmentally friendly and energy-efficient resource management.

Anaerobic digestion (AD) dewatering liquor is wastewater produced through the dewatering process of solid digestate (i.e., AD sludge) emitted from the AD treatment of organic waste. This liquor poses a severe contamination risk because it usually contains high organic and nutrient concentrations as well as >500 mg-N/L of total ammonia nitrogen (TAN), which refers to the amount of nitrogen present as NH_3 and NH_4^+. Biological nitrification and denitrification of TAN is challenging because AD dewatering liquor contains non-biodegradable organic materials (Zhao et al., 2015). Moreover, N_2O gas, which has a global warming potential 300 times higher than that of CO_2, is also produced

* Corresponding author.
E-mail addresses: kangjeonghee@kict.re.kr (J.-H. Kang), ohgg0404@kict.re.kr (G.-G. Oh), smson03@ktl.re.kr (M. Son), kangsw93@kict.re.kr (S. Kang).

https://doi.org/10.1016/j.jenvman.2025.126661
Received 22 April 2025; Received in revised form 1 July 2025; Accepted 16 July 2025
Available online 22 July 2025

(Im et al., 2025). Therefore, it is necessary to alleviate the influence of ammonia on the environment.

TAN recovery and utilization, instead of the removal to innocuous nitrogen gas, is regarded as an important strategy to alleviate environmental threats, and recently, various technologies concerning TAN recovery have been developed and applied. Stripping and struvite precipitation have been applied, owing to their technological maturity (Tian et al., 2019). Membrane-based processes—membrane distillation, osmotic distillation, and electrodialysis—offer high selectivity for TAN without by-products such as sludge (Im et al., 2025). However, these approaches have several drawbacks, including high operational costs, relatively low efficiency, and intricate operations (Dai et al., 2024). Conversely, ion exchange is a reliable initiative that offers low energy consumption, straightforward operation, and outstanding removal efficacy. Because of these advantages, ion exchange has been employed for heavy metals, natural organic matter, and nutrient removal, in addition to TAN recovery (Lizarralde et al., 2021). Nonetheless, a critical concern associated with the disposal of highly concentrated regenerant brines containing condensed contaminants (e.g., TAN) remains.

For highly selective ion exchange materials, Prussian blue analogs (PBAs) are well known for their excellent adsorption of monovalent cations such as Cs^+, Ti^+, and NH_4^+ (Zhang et al., 2025). Following an earlier study by Kang et al. (2023), a copper-based PBA was prepared and used as an adsorbent to recover TAN. In a subsequent study, a bipolar membrane (BPM)-integrated electrolytic cell was developed (Kang et al., 2024). Electrochemical oxidation of ammonia proceeds under alkaline condition, necessitating the maintenance of the solution pH > 9.0 to sustain the reaction. Due to unshared electron pair of free ammonia (:NH_3), it is more favorably adsorbed onto the anode surface and undergoes oxidation more efficiently than its conjugate acid, the ammonium ion (Bunce & Bejan, 2011). However, ammonia oxidation consumes OH^- resulting in a decrease in pH. BPM provides OH^- ion to the anodic chamber via the dissociation of H_2O to H^+ and OH^- under reverse bias condition (Han et al., 2022). Continuous provision of OH^- assists in sustaining alkaline condition. As a strategic approach, a system coupled with TAN recovery using PBA and conversion to hydrogen gas via electro-oxidation was investigated.

The use of this coupled system of ion exchange and electro-oxidation is not entirely new. Gendel and Lahav introduced a process comprising cation exchange resin and subsequent electrochemical regeneration to remove TAN in a fishpond (Gendel and Lahav, 2013). They used commercial chabazite for the ion exchange and a 50 g Cl^-/L solution as a regenerant. However, hydrogen production and changes in adsorption capacity resulting from the long-term usage of ion-exchange resins were not discussed in the literature. A similar approach was reported by Li using zeolite (Li et al., 2009). In the study, changes in the adsorption capacity were examined through five repeated tests. Although no changes in the adsorption capacity and reusability of ion exchange resins over many cycles have been reported, those experiments were conducted using artificial wastewater, which contains no competing cations. Since various interfering ions coexist in actual wastewater, it is essential to monitor changes in adsorption performance and identify potential causes of degradation. In particular, long-term stability through repeated use is necessary to evaluate practical applicability. However, to the best of our knowledge, this has not yet been reported.

Many studies on the electro-oxidation of TAN have been conducted in undivided cells to enhance the removal rate. A study by Lahav et al. demonstrated the stability of ion-exchange capacity despite repeated use over 68 cycles; however, electro-oxidation for regeneration was performed using an undivided cell (Lahav et al., 2013). More recently, a study on the electrolysis of TAN in a divided cell was reported by Kuang et al. (2022). In this study, TAN in raw landfill leachate was electrolyzed without a separate TAN recovery process. Since TAN was oxidized with the assistance of Cl^- present in the leachate, corrosion of the membrane or electrodes may have occurred as a result of residual chlorine. In contrast, TAN oxidation in a NO_3^- solution via direct oxidation can prolong the lifespan of the electrolyzer. However, direct oxidation of TAN is difficult to achieve because of the requirement for alkaline conditions. A rapid pH decrease in the anolyte suppresses direct electro-oxidation. Finally, a simultaneous evaluation of the technical and economic feasibility of a coupled ion-exchange and electrolysis system has rarely been reported.

This study proposed a coupled system with ion exchange and electro-oxidation techniques using TAN as a crucial hydrogen carrier. We aimed to assess the technical viability and economic feasibility of the proposed system through a series of experiments and economic calculations. To estimate technical viability, a single-cycle experiment, repeated twelve times, was designed in which adsorption, desorption (i.e., regeneration of the adsorbent), and electrolysis were performed sequentially. The short-term stability of the system was confirmed by observing the changes in the adsorption capacity, TAN recovery rate, and electro-oxidation rate. Finally, capital expenditure (CAPEX) and operational expenditure (OPEX) associated with the upscaled system were assessed to evaluate its economic feasibility.

2. Materials and methods

2.1. Materials

The adsorbent, in which PBA is immobilized, was produced using a weakly acidic cation exchange resin (Samyang Ltd., Korea), $CuSO_4 \bullet 5H_2O$ and $K_4Fe(CN)_6 \bullet 3H_2O$ (99.0 %, Samchun Chemical Reagent Co. Ltd., Korea), and deionized water. The preparation method for the adsorbent is detailed in a previous study (Kang et al., 2023). The regenerant was prepared by dissolving 1 mol KNO_3 (99.9 %, Daejung, Korea) in deionized water of 1L.

The AD dewatering liquor for batch and column tests was collected from a local wastewater treatment plant in Goyang-si, Korea. The liquor discharged from the centrifugal dewatering process was taken and used after filtration to prevent blockage of the adsorbent column by suspended particles in the liquor. Filtration was performed using a GF/C filter and a vacuum pump. Notably, no changes in the physicochemical properties of the liquor were observed after filtration. The AD dewatering liquor was refrigerated and then used after raising the temperature to room temperature (~22 °C). The detailed chemical composition is listed in Table S1. Various ions were present in the dewatering liquor. Cations such as K^+, Na^+, Ca^{2+}, and Mg^{2+}, which may compete with TAN for adsorption, were present. The TAN concentration was 482.67 mg/L.

2.2. Isotherm & kinetic study

Isotherm and kinetic experiments were performed to elucidate the adsorption properties of PBA. The amount of TAN adsorbed per gram of PBA was calculated using Eq. (1).

$$q_e = \frac{(C_0 - C_e)}{m \cdot V} \quad (1)$$

where, q_e is the adsorption capacity at equilibrium (mg-N/g), C_0 is the initial TAN concentration (mg-N/L), C_e is the equilibrium concentration after adsorption (mg-N/L), m is the adsorbent weight (g), and V is the volume of the solution (L).

2.2.1. Isotherm study

Isotherm tests were conducted to evaluate the adsorption equilibrium of the PBA. To determine equilibrium, 0.01, 0.02, 0.04, 0.08, and 0.2 g of PBA were placed in a polypropylene conical vial with a volume of 50 mL. The AD dewatering liquor (20 mL) was added to the vials and allowed to react for 24 h. Vials in which no PBA was placed were prepared as blank tests. The initial TAN concentration was 500 ± 25 mg-N/L, and the PBA doses were organized in triplicate for the analyses. The adsorption mechanism and capacity were characterized using Langmuir

(Eq. (2)), Freundlich (Eq. (3)), and Temkin (Eq. (4)) equations as follows:

$$\text{Langmuir}: q_e = q_m \frac{a_L C_e}{1 + a_L C_e} \quad (2)$$

$$\text{Freundlich}: q_e = K_F C^{1/n} \quad (3)$$

$$\text{Temkin}: q_e = \frac{RT}{b} \ln (K_T C_e) \quad (4)$$

where q_e is the quantity of adsorbate adsorbed on the PBA (mg-N/g); q_m is the maximum sorption capacity of the adsorbent (mg-N/g); C_e is the equilibrium concentration of the adsorbate in solution (mg-N/L); a_L is the Langmuir affinity constant (L/mg-N); K_F and 1/n are constants that indicate the adsorption capacity and intensity, respectively; R is the universal gas constant (8.314 J/mol•K); T is the absolute temperature (K); b is the Temkin constant (J/mol); and K_T is the adsorption equilibrium constant (L/g-N).

2.2.2. Kinetic study

Adsorption kinetic experiments were conducted to understand the effect of reaction time on the removal efficacy of PBA. PBA (20 mg) was placed in 50 mL vials and kept in a shaking incubator (22 °C) for 24 h. The TAN concentration was measured at the reaction times of 1, 3, 5, 10, 30, 60, 120, 240, 480, and 1440 min. Three separate vials were used to obtain average concentrations and standard deviations. Several kinetic models, defined by Eqs. (5)–(8), were used to analyze and interpret the experimental data as follows:

$$\text{Pseudo first} - \text{order}: q_t = q_e\left(1 - e^{-k_1 t}\right) \quad (5)$$

$$\text{Pseudo second} - \text{order}: q_t = \frac{k_2 q_e^2 t}{1 + k_2\, q_e t} \quad (6)$$

$$\text{Elovich}: q_t = \left(\frac{1}{b}\right) ln(ab) + \left(\frac{1}{b}\right) ln\,(t) \quad (7)$$

$$\text{Intra} - \text{particle diffusion}: q_t = K_p t^{\frac{1}{2}} + C \quad (8)$$

where, q_t (mg-N/g) is the amount of TAN adsorbed at a given time t; q_e is the equilibrium adsorption uptake extrapolated from the experimental data at an infinite time (mg-N/g); k_1 (h^{-1}) and k_2 (g/mg-N•h) are the rate constant of the pseudo first and second order, respectively; and K_P (mg-N/g•$min^{0.5}$) is the rate constant for intra-particle diffusion.

2.3. Adsorption, regeneration, and electrolysis

2.3.1. Reactors

Fig. 1 illustrates the schematic of the experimental design. The adsorption column was prepared using a Plexiglas cylinder with an inner diameter of 10 mm and a height of 200 mm. The column was filled with PBA adsorbent of 4.25 g and the packing density was 270 g/L. An electrolyzer—consisting of two chambers—was fabricated using Plexiglas. The chambers were separated using a bipolar membrane (Astom Corporation, Shunan, Japan). Each chamber held 150 mL of electrolyte, with internal dimensions of 50 × 50 × 60 mm. However, the working volume in the anodic and cathodic chambers was adjusted to 140 mL to provide headspace. Commercial electrodes (DE NORA PERMELEC Ltd., Fujisawa, Japan) were used as anode and cathode. These electrodes consisted of titanium mesh coated with platinum, with a geometric surface area of 15 cm^2. The electrodes and membrane were secured using a silicon gasket. The distance between the electrodes and the BPM was maintained at 1 mm, determined by the thickness of the silicon gasket. The electrolyzer assembly was completed using a stainless-steel plate, which simultaneously applied pressure to both chambers. Electrolysis was conducted at room temperature (25 ± 1 °C), and no chiller was employed. Teflon Gasbags were connected to the electrolyzer at the top of each cell to exhaust gas emissions, and a magnetic stirrer was placed in each cell to agitate the electrolyte. Detailed information on the electrolyzer configuration is described in a previous study (Kang et al., 2024).

2.3.2. Experimental procedure

1) ***Adsorption stage***: The AD dewatering liquor was introduced into the column at a flow rate of 1.0 mL/min, corresponding to an empty bed contact time of 15 min. The flow rate was regulated using a peristaltic pump (Masterflex, USA). Effluent samples were collected at 30-min intervals throughout the adsorption experiment to determine the concentration of total ammonia nitrogen (TAN). Subsequently,

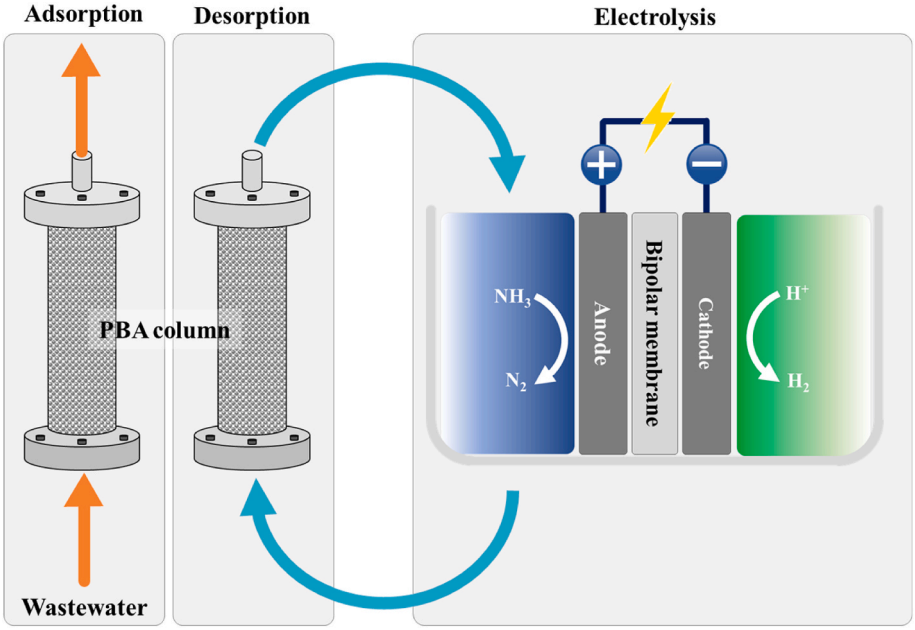

Fig. 1. Experimental design schematics.

the column was drained with compressed air for a few seconds to minimize contaminant transfer to the regenerant (1 M KNO_3 solution).

2) ***Desorption stage***: After drainage, the regenerant was passed through the column with 1.0 mL/min for desorption of TAN on PBA. The discharged regenerant was used for the analysis, and the remainder was collected in a reservoir. Subsequently, the column was drained using compressed air for a few seconds. The volume of the drained regenerant was <1 mL, which was negligible compared with the total volume (360 mL) used for desorption.; thus, the drained regenerant was wasted.
3) ***Electrolysis stage***: The pH of the regenerant collected in the reservoir was adjusted to 13.0 by adding KOH tablets. After adjustment, the regenerant was transferred to the anodic chamber of the electrolyzer. The cathodic chamber was filled with catholyte (1 M KOH). Electrolysis performance and variation were investigated by comparing TAN removal efficacy. Accordingly, a fixed direct current of 1.2 A, corresponding to 80 mA/cm^2, was applied using a DC power supply (DP30-03C, TOYOTECH, Korea) for TAN electro-oxidation in the regenerant. The solutions were stirred vigorously during electrolysis. During desorption and electrolysis, loss of regenerants inevitably occurs as a result of analysis and drainage. Accordingly, a new regenerant was added to increase the total volume of the regenerant to 360 mL. However, it should be noted that the volume of the new regenerant added was <20 mL in every cycle; therefore, chemical property shifts resulting from the addition of new regenerant were disregarded. The electrochemically treated regenerant was then used to desorb TAN in the next desorption stage. The three-stage experiments were repeated for 12 cycles.

2.4. Analytical method

The TAN concentration was quantified using a Nessler reagent with an ultraviolet–visible spectrophotometer at 420 nm (DR5000, Hach, USA). The pH was measured using a portable instrument (SG98, METTLER TOLEDO, USA). The ions in the wastewater were analyzed using ion chromatography (Dionex Aquion, Thermo Fisher Scientific, USA). Scanning electron microscopy combined with energy-dispersive X-ray spectroscopy (SEM-EDS) was used for surface analysis (JSM-7001F, JEOL Ltd., Japan).

3. Results and discussion

3.1. Isotherm and kinetic study

Adsorption isotherm tests were conducted to quantify the maximum adsorption capacity (q_{max}). Fig. 2 (a) shows the isotherm test results along with model fitting. As summarized in Table S1, multiple coexisting ions potentially compete with ammonium for adsorption sites. This ionic competition can lead to fluctuations in ammonium adsorption capacity. Nevertheless, the adsorption behavior remained consistent, as evidenced by the minimal variation observed across triplicate experiments.

The relative standard deviations (RSD), calculated using Eq. (S1), were <5 %, which is generally considered statistically acceptable. Therefore, the mean values can be used to describe the TAN adsorption characteristic of PBA. The q_{max} value based on equilibrium in the experimental results was 59.08 mg-N/g. The q_{max} had considerable value in comparison with that of other studies. Nativ et al. reported 26.26 mg/g of PES-ZnHCF for the treatment of wastewater from live seafood transportation (Nativ et al., 2021). Although the highest value was 93.00 mg/g, PBA was a powdered material (Parajuli et al., 2016).

The adsorption isotherm curves of ammonium exhibited a better fit to the Langmuir adsorption characteristics compared to the Freundlich model, evidenced by the higher correlation coefficient (R^2). These results suggested that ammonium adsorption involves monolayer adsorption at the activated sites on the adsorbent surface and reversible

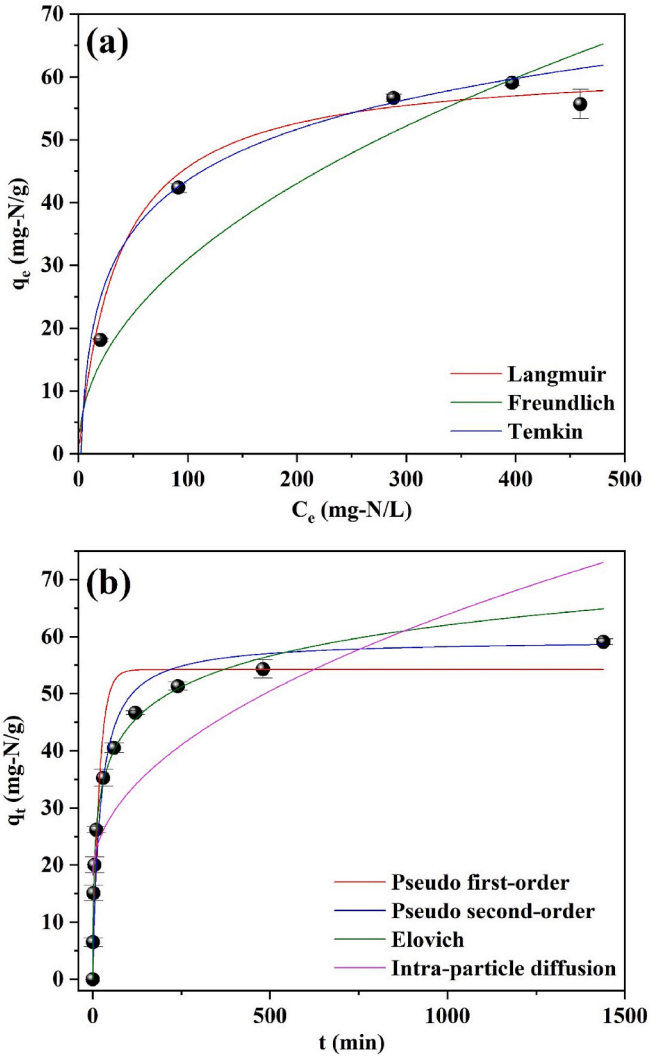

Fig. 2. Ammonium adsorption (a) isotherm test and (b) kinetic test result at 295 K. Retention time: 24 h, pH: 6.8. (Colored lines are the fitting curves and error bars indicate the standard deviation of the triplicated experiment).

chemisorption (Nativ et al., 2021). In a previous study, we evaluated the adsorption capacity through an isotherm test using synthetic wastewater prepared with NH_4Cl and deionized water (Kang et al., 2023). The TAN concentration in synthetic wastewater was identical to that in this study, showing a strong correlation with the Langmuir model. This demonstrated that ammonium was preferentially adsorbed on the PBA, regardless of the coexistence of abundant competing ions in actual wastewater. Although the Freundlich model exhibited a weaker correlation than the Langmuir model (R^2 = 0.8972), the parameters confirmed that ammonium adsorption onto PBA was related to its strong intensity and high affinity (Table 1).

According to the correlation coefficient, The Temkin model fitted the experimental results well (R^2 = 0.9945). Because the Temkin model assumes electrostatic interactions between adsorbates and adsorbents, the molecular heat of adsorption decreases linearly with the coverage of PBA-activated sites (Fan et al., 2017; Ma et al., 2020). This was consistent with the Langmuir isotherm results; therefore, it was supposed that the adsorption process may be caused by reversible ion exchange. Furthermore, the adsorption characteristics enable the selective adsorption of ammonium, even under competition with other ions.

Adsorption kinetic studies are useful for understanding adsorption rates and diffusion mechanisms. The kinetic test data were also statistically significant, with RSD of <5 % across triplicate experiments. The

Table 1
Kinetic and isotherm model parameters.

Models		Parameters			
Isotherms	Langmuir	R^2	a_L (L/mg-N)	–	q_e (mg-N/g)
		0.9917	0.028	–	62.15
	Freundlich	R^2	K_F ((mg-N/g)(L/mg^{-1})$^{1/n}$)	1/n (dimensionless)	–
		0.8972	3.475	0.475	–
	Temkin	R^2	B (J/mol)	K_T (L/g-N)	–
		0.9945	210.3	0.42	–
Kinetics	Pseudo first-order	R^2	k_1 (1/min)	–	q_e (mg-N/g)
		0.9289	0.028	–	62.11
	Pseudo second-order	R^2	k_2 (g/mg-N•min)	–	q_e (mg-N/g)
		0.9701	0.0008	–	59.45
	Elovich	R^2	a_E (mg-N/g•min)	b_E (g/mg-N)	q_e (mg-N/g)
		0.9916	22.13	0.13	64.86
	IPDM	R^2	K_i	C	q_e (mg-N/g)
		0.6929	1.45	18.16	73.01

TAN adsorption rate increased rapidly from the onset to 60 min, and then approached adsorption equilibrium after 500 min (Fig. 2(b)). This was because of the high initial TAN concentration in the solution. At the onset, the abundant adsorption sites on the PBA surface facilitated the rapid adsorption of TAN at the adsorption sites (Parajuli et al., 2016). As adsorption continued, the TAN concentration and available adsorption sites decreased, resulting in a gradual removal rate decrease. Finally, the TAN adsorption process reached saturation, and the maximum experimental amount of TAN adsorbed was 59.08 mg-N/g. The experimental results were analyzed using kinetic models to identify the adsorption characteristics of TAN onto PBA.

The results fitted to the kinetic models are described in Fig. 2(b). According to the pseudo first- and second-order fitting results, the pseudo second-order model was superior in interpreting the experimental points in the kinetic experimental results. The R^2 values of the pseudo first- and second-order models were 0.9289 and 0.9701, respectively (Table 1). The maximum adsorption capacity of the pseudo second-order model (58.60 mg-N/g) was closer to the experimental value (59.08 mg-N/g) than that of the pseudo first-order model (62.11 mg-N/g). This indicated that the pseudo second-order model adequately described the experimental data. The pseudo-first-order kinetic model is typically effective in describing adsorption behavior during the initial phase, particularly within the first 30 min, whereas the pseudo-second-order model provides a better fit for representing the adsorption kinetics over the entire duration of the process (Ahn et al., 2022). This study agreed with reports showing an identical interpretation of pseudo first-order kinetics with experimental data in 30 min. In addition, the results fit well with a pseudo second-order regression. Moreover, the pseudo first-order model assumes that physisorption is the main adsorption mechanism and the resistance to mass transfer in the sorbent is the limiting factor. In contrast, the pseudo second-order model presumes chemisorption on the active sites on the sorbent surface (Sumalinog et al., 2018; Ahn et al., 2022). This demonstrates that the chemical reaction on the PBA surface was the main adsorption mechanism, consistent with the isotherm findings.

The Elovich model is typically used to describe the adsorption process (Nguyen et al., 2022). As shown in Fig. 2(b), the Elovich model well described the experimental points demonstrating the interaction between ammonium and the sorption sites based on the model assumptions. Additionally, the constants a_E and b_E in the Elovich equation are associated with the chemisorption rate and surface coverage, respectively (Largitte and Pasquier, 2016). The calculated values are listed in Table 1 ($a_E = 22.23$, $b_E = 0.13$). Compared with other literature data (Table S2), the PBA in this study had a lower a_E and higher b_E. This implied that the PBA adsorption rate was slower, but the adsorption capacity was higher than that of the other adsorbents. Eq. (8) can be modified to Eq. (9) using assumptions and simplifications (Wu et al., 2009) as follows:

$$\frac{q_t}{q_{ref}} = R_E \ln\left(\frac{t}{t_{ref}}\right) + 1 \quad (9)$$

where, t_{ref} is the longest time in the adsorption process, q_{ref} is the adsorbate uptake at adsorption time t_{ref}, and R_E is a coefficient related to the adsorption rate. According to the classification of Wu et al., the adsorption curve was zone II (R_E = 0.12) with a "mildly rising" adsorption curve (Wu et al., 2009). The literature noted that the chemical adsorption process typically exhibits a zone II curve.

Unlike other kinetic models, the Intra-particle diffusion model exhibited poor fitting results ($R^2 = 0.6929$). The plot of q_t versus $t^{1/2}$ in Fig. S1 shows three linear sections, indicating that intra-particle diffusion is involved in two or more steps governing the adsorption process (Inyinbor et al., 2016). Correspondingly, the hysteresis plot exhibits a typical type III adsorption-desorption form, indicating abundant mesopores (Fig. S2). Adsorbent micropores are covered by PBA (Kang et al., 2023; Thommes et al., 2015); therefore, the adsorption amount can be maximized by operating under a sufficient contact time (or slow flow rate) due to adsorption sites in intra-particle pores.

3.2. Column test

From the isotherm and kinetic tests, it was confirmed that PBA allowed the selective adsorption of TAN via chemical adsorption and ion exchange, despite competing cation coexistence. In the column test, the practical feasibility and short-term stability of PBA were evaluated through the continuous use of PBA and the regenerant. Changes in the adsorption capacity and desorption efficiency were observed and are discussed in this chapter; thereafter, the results of the electro-oxidation treatment of the regenerant are reviewed in the following chapter. Fig. 3 (a) shows the breakthrough curves obtained from column tests over 12 cycles. In the first cycle test, the removal efficiency decreased by <20 % after 12 h (black square points); thereafter, a stationary phase was observed, indicating near saturation. Thus, we posited that the adsorption capacity was exhausted after 16 h operation, and a fixed operation time of 16 h was used to compare the adsorption capacities in each cycle.

The removal rate of TAN decreased by <20 % after 16 h in the first cycle, whereas it was >30 % after the second cycle, implying an enhancement in the adsorption capacity. PBA possesses two types of adsorption sites—interstitial and vacancy sites. At the interstitial sites, TAN is adsorbed to replace K^+ in the PBA crystal structure. In contrast, TAN reacts with water molecules adsorbed at the vacancy site surrounded by six open metal sites as follows (Usuda et al., 2022):

$$PBA{\bullet}nH_2O + mNH_3 \rightarrow PBA{\bullet}(n\text{-}m)H_2O{\bullet}mNH_3 + mH_2O \quad (10)$$

When PBA was prepared, the vacancy sites did not combine with water molecules. During the first operation cycle, water molecules were held at the vacancy sites (i.e., activation); therefore, the adsorption capacity increased because of the generation of additional adsorption sites.

The breakthrough curves were analogous trends, except in the first cycle (Fig. 3(a)). This demonstrates that the adsorption capacity was maintained without PBA deterioration, despite the introduction of actual wastewater. The critical mechanism for the decrease in the adsorption capacity of the adsorbents is the irreversible adsorption of competing cations dissolved in the wastewater. However, PBA was not influenced by the cations, demonstrating its excellent feasibility for

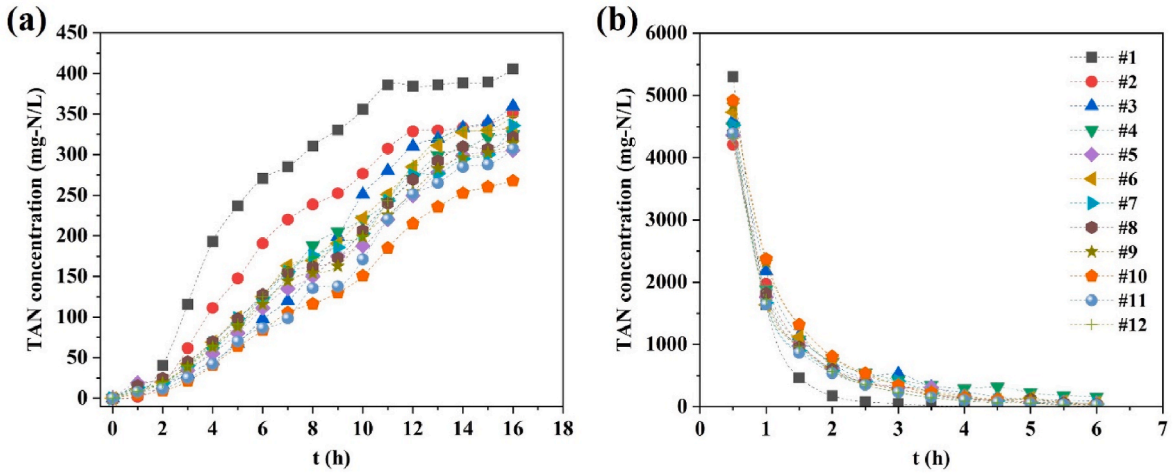

Fig. 3. The concentration profiles of adsorption (a) and desorption (b) as a function of time.

practical applications. The desorption curves presented almost identical concentration profiles in each experiment as compared to the adsorption curves, even in the first cycle. The regenerant was prepared using deionized water and chemicals, and the reaction rates were similar. The constant desorption efficacy was also a result of the exclusive adsorption and desorption characteristics of PBA, which affected the stable operation of the electrolyzer.

An effluent concentration of 4000–5000 mg-N/L was observed after 1 h, after which it decreased sharply to 800 mg-N/L after 2 h (Fig. 3(b)). The desorption curves exhibited a pseudo first-order reaction. Owing to the steady introduction of regenerants containing high concentrations of K^+, the desorption rate was only influenced by the amount of TAN adsorbed on the PBA, suggesting a pseudo first-order reaction. Given the desorption curve and findings, most of the TAN adsorbed on the PBA was transferred into the regenerant within 3 h. A higher concentration is favorable for the electro-oxidation of TAN in terms of the energy efficiency of the electrolyzer. Hence, the desorption time should be determined simultaneously by considering the desorption rate and energy efficiency.

The masses of the adsorbed and desorbed TAN for the full cycles were calculated (Fig. 4). The total amount of adsorbed and desorbed TAN varied from 296 to 348 mg, except in the first cycle, and 278–352 mg, with averaged values of 332.3 ± 14.8 and 312.1 ± 23.1 mg, respectively. The recovery rate ranged from 87.6 to 100 % with a mean value of 94.3 ± 5.5 %. In addition to the adsorption/desorption curves shown in Fig. 3, the recovery rate also demonstrates that there was no deterioration in the removal capacity of TAN. Moreover, the regenerant showed stable desorption properties despite continuous usage. According to a report (Nativ et al., 2022), a PBA had a TAN recovery rate of >95 % in artificial wastewater composed of distilled water and chemicals; however, it decreased to 88 % when real wastewater was used because of competing cations (Na^+ and K^+). Likewise, this study showed a mean recovery rate of 93.9 ± 6.1 %, indicating compatible ability with other adsorbents.

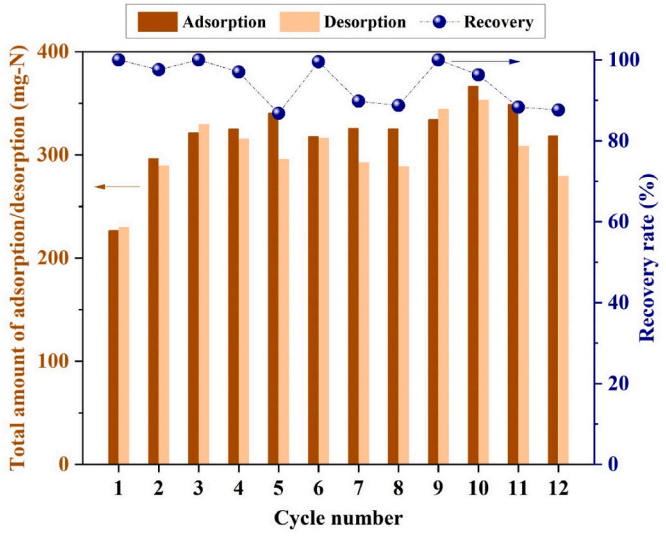

Fig. 4. The total amounts of adsorbed and desorbed ammonia in twelve cycles of adsorption and desorption followed by electrochemical generation (Brown colored bar: adsorption, skin colored bar: desorption, scatter point: recovery rate).

Apparently, PBA exhibited a steady TAN recovery ability over 12 cycles. However, undesirable ions could be irreversibly adsorbed, particularly divalent cations (Ca^{2+} and Mg^{2+}), owing to the electrostatic affinity of PBA. Accordingly, the surface of the adsorbent used for 12 cycles was examined using SEM-EDS. Table 2 shows the proportions of the elements corresponding to the SEM-EDS analysis of the PBA surface before use (pristine), after a 12-cycle adsorption, and after a 12-cycle desorption. In contrast to pristine PBA, the relatively high O element content after use indicates that PBA has a high coordination water content, suggesting a high ammonia adsorption capacity (Li et al., 2025). As mentioned above, some water molecules combine with the vacancy site, which has a potential TAN adsorption ability. The SEM-EDS data are in accordance with this theory.

Regardless of the usage, carbon was the most abundant element, resulting from the carboxyl functional groups in the weakly acidic cation and cyan groups in PBA. The percentage of K varied notably depending on PBA utilization. The pristine and adsorbed PBA had ~15 % K ions, which increased to 24.86 %, indicating ion exchange between the adsorbed TAN and K^+ in the regenerant. The Fe and Cu percentage decreases were caused by the relative decline resulting from the increase

Table 2
Changes in the adsorbent weight percentage from SEM-EDS detection after a 12-cycle operation.

Element	Pristine	Adsorption	Desorption
C	46.08	39.42	47.62
O	10.18	21.83	19.75
N	11.12	9.63	3.36
K	14.63	15.21	24.86
Fe	10.48	4.01	2.38
Cu	7.30	3.19	1.70
Mg	0.21	0.59	0.33
Ca	N.D	6.12	N.D

in K and O, rather than the deterioration of PBA. Unlike the pristine sample, Ca adsorption was observed after the adsorption process, indicating an undesirable side reaction. However, Ca was no longer detected after desorption, suggesting that the PBA used in this study can be readily applied in wastewater treatment. Based on SEM-EDS analysis, no noticeable changes were observed on the PBA surface. In addition, the structural stability of the PBA was confirmed by XPS analysis, as shown in Fig. S3. The major constituent elements showed minimal variation even after 12 cycles of use.

3.3. Regenerant electrolysis

In the previous section, changes in the adsorption capacity of PBA were examined through continuous adsorption and desorption tests to determine their practical feasibility. PBA effectively recovered TAN from real wastewater. The withdrawn TAN should be removed to ensure the continuous use of the regenerant. Here, electrolysis was investigated as a sustainable technology for utilizing TAN. The characteristics of the electro-oxidation of the regenerant and changes in the chemical properties were investigated to estimate its stability along with that of PBA. Before analyzing the TAN concentration profiles, it is important to note that the linear sweep voltammogram showed a decrease in peak current in the range of 1.6–1.7 V, as shown in Fig. S4. Furthermore, the TAN removal efficiency declined as the current density decreased (Fig. S5). Ultimately, around 8.5 % of the ammonia removed was transformed into nitrate (Fig. S6). These results verify that TAN electro-oxidation was effectively achieved in the electrolytic cell developed in this study. The average electric conductivity of the regenerant over 12 cycles was 34.2 ± 0.3 mS/cm before electrolysis. After electrolysis, it decreased to 32 ± 0.4 mS/cm, indicating TAN removal. The cell voltage ranged from 7.2 to 7.8 V throughout electrolysis, demonstrating stable operation of the electrolytic cell and minimal changes in the regenerant composition.

Fig. 5(a) illustrated the TAN concentration changes during electrolysis of the regenerant at the first cycle. The TAN concentration profiles showed statistically significant results, with RSD below 5 % across triplicate measurements. The TAN concentration decreased linearly with electrolysis time, indicating zero-order kinetics. In general, the direct oxidation regime is dominant in electrolysis cells without anions, which can electrochemically generate oxidants such as Cl^- and SO_4^{2-}. In a direct electro-oxidation process, pseudo first-order oxidation kinetics are common because of the relatively low diffusion to the electrode surface compared to the oxidation rate, which is the rate-limiting step. Notably, NO_3^- was used as the electrolyte, which produces no oxidants, indicating that direct oxidation is the predominant pathway. Therefore, the observation of pseudo-first-order kinetics is reasonable. Nevertheless, the nearly linear oxidation rate suggests that factors beyond electrochemical oxidation may contribute to the overall process.

Two factors may influence the discrepancy between anticipation and results. The first factor is stripping resulting from the temperature increase. Mass balance on electro-oxidation of the regenerant is described in Fig. S6. A decrease of 118 mg-N/L, accounting for 8.6 % of the total concentration, occurred even without electro-oxidation. Additionally, during electro-oxidation, nitrogen gas is produced from TAN and subsequently released into the atmosphere.

High temperatures also accelerate TAN stripping; Therefore, ammonia volatilization under strongly alkaline conditions significantly contributes to the overall removal rate. Another potential factor is the thermal effect because a chiller for the electrolyzer was not employed. When the initial water temperature was 22 °C (i.e., room temperature), it increased to >65 °C at the end due to the joule heat from electrode. It is well defined by the Arrhenius equation that an increase in temperature promotes chemical reactions. In conclusion, the oxidation rate varied due to external factors and the pseudo first-order reaction was not observed.

Diffusion from the anolyte to the catholyte through the BPM was possible because free ammonia is uncharged. However, a TAN concentration of less than 1 mg-N/L was observed in the catholyte after electrolysis, indicating that TAN loss resulting from diffusion was negligible. This is attributed to the very low TAN concentration, which was insufficient to drive significant diffusion. Therefore, TAN loss through diffusion toward the catholyte may occur only when the TAN concentration in the anolyte is relatively high.

The TAN concentration decreased to <30 mg-N/L after 270 min of electrolysis (Fig. 5(a)). The current efficiency of the electrolyzer, calculated using Eq. (S2), was 21.07 %. This relatively low value is attributed to the high applied current density of 80 mA/cm^2. In a previous study, a current efficiency of 30.4 % was achieved under an optimized current density of 60 mA/cm^2 (Kang et al., 2024). However, since hydrogen gas production is directly proportional to the applied current, the operating current in the proposed system should be selected by balancing the current efficiency and hydrogen production.

In a preliminary test, it was confirmed that a concentration of <30 mg-N/L was sufficient to desorb the TAN adsorbed in PBA without influencing the desorption rate (data not shown). Consequently, the TAN concentration was determined after electrolysis for 270 min in subsequent experiments (2–12 cycles). As shown in Fig. 5(b), the concentration varied from 23 to 28 mg-N/L after electrolysis, implying an analogous electro-oxidation rate to that shown in Fig. 5(a). Therefore, it

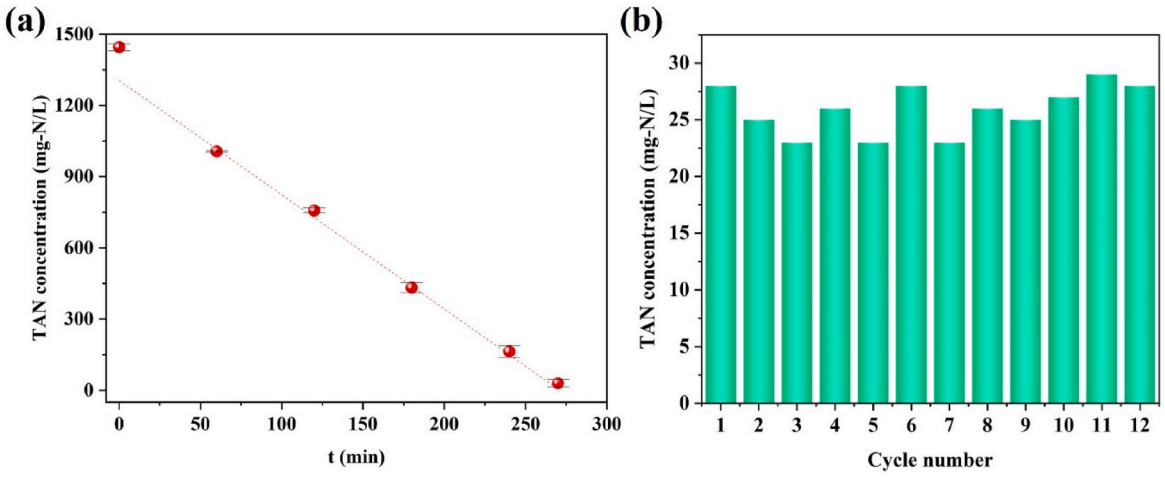

Fig. 5. TAN concentration changes of the regenerant as a function of time (a) and with respect to operation cycles (b). The dashed line indicates linear regression. The error bars indicate the standard deviation of the triplicated measurement.

can be assumed that the chemical properties of the regenerant were constantly sustained and consistent with the desorption curve shown in Fig. 3(b).

In addition to the oxidation rate, ion concentration was used as a supplementary index to assess the stability of the regenerant. K^+ is a key element because TAN is recovered from the regenerant via ion exchange. NO_3^-, which is a crucial pollutant, is possibly generated during the electro-oxidation of TAN and accumulated as the system operates continuously. Therefore, the regenerant must be replaced with a fresh solution at a given period. Fig. 6 depicts the concentration changes of K^+ and NO_3^-. The concentration of K^+ (red circle) in the first cycle decreased from 1.0 to 0.94 M and increased steadily thereafter. KOH was added to create alkaline conditions, essential for direct electro-oxidation before electrolysis. Hence, the concentration of K+ increased constantly with continuous regenerant usage.

NO_3^- concentration—originating from the electro-oxidation of TAN—also increased continuously, albeit more insignificantly than K^+. In a direct oxidation regime, nitrogen gas is the most common end-product. However, NO_3^- can be generated as follows (Liu et al., 2024):

$$NH_3 + 9OH^- \rightarrow NO_3^- + 6H_2O + 8e^- \quad (11)$$

The conversion rate to NO_3^- generation is unprevailing because it requires a high oxidation potential and eight electrons. This implied that the regenerants can be used repeatedly for a long time, and the change period must be estimated through a long-term experiment.

Finally, hydrogen gas was consistently produced during the electrolysis of TAN in the cathodic chamber, with a purity of 95 %. The energy efficiency associated with hydrogen production, calculated using Eq. (S3), was 31 %, indicating partial recovery of the total energy consumed for ammonia removal. This value is typical for operations conducted at high voltage and low current density (Cho and Hoffmann, 2017). Based on the results obtained in this study, hydrogen gas was successfully produced, comparable to that of a conventional electrolyzer. Moreover, the BPM has a bilayer structure in which cation and anion exchange layers are in contact. By means of structural features, the gas electrochemically generated in the anodic chamber (O_2, N_2) scarcely penetrate to cathodic chamber, and vice versa. This characteristic of the BPM was advantageous as it can obtain pure hydrogen gas along with OH^- generation. In conclusion, TAN removal and hydrogen gas were successfully achieved using the proposed system.

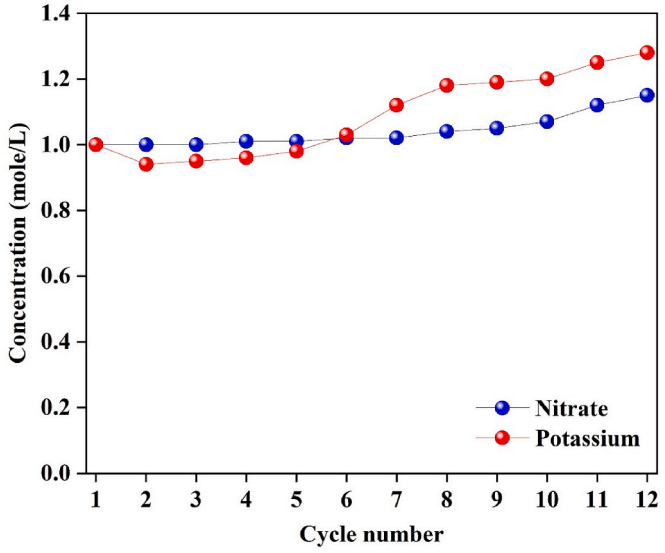

Fig. 6. Changes in the concentrations of nitrate and potassium ions in the regenerant after electrolysis.

3.4. Economic assessment of the proposed system

To determine the economic feasibility of the proposed system, the capital and operational expenditures (CAPEX and OPEX) were estimated based on operational standpoints, current literature information, and assumptions. An exchange rate of 1450 Korean won per U.S dollar ($) was applied to present the cost as $. The CAPEX comprises an electrolyzer, two adsorbent towers, installation, a pipeline, utilities, and civil. The costs of the electrolyzer and adsorption tower construction were calculated using the cost exponent defined in Eq. (12) (Lee et al., 2017):

$$\frac{C_a}{C_b} = \left(\frac{A_a}{B_b}\right)^{0.6} \quad (12)$$

where, C is the purchase cost, A and B are the equipment, and 0.6 is the cost exponent based on a sixth–tenth rule that shows a good approximation for estimating the cost of upscaled equipment (Lee et al., 2017). Assuming a 1000 m^3/d AD effluent flow rate as a model facility for estimating CAPEX and OPEX, a 2835 kg adsorbent is required with a 10 min empty bed contact time, 270 g/L packing density, and 0.7 m^3 bed volume from the experimental data. The purchase prices of the electrolyzer and the adsorbent tower were supposed to be 0.398 and 0.232 M$, respectively (Table 3). It should be noted that the CAPEX of an electrolyzer system encompasses the stack, balance of plants, power electronics, civil, utilities, and pipelines because of their small contributions to the system (Krishnan et al., 2023).

The OPEX comprises electricity, water, labor, maintenance, chemicals (NaOH and $NaNO_3$), and other operating costs. The grid electricity price was fixed at 0.12 $/kWh, and the operating labor cost was estimated assuming two workers operating in three shifts daily, with a 37 $/h cost. The maintenance and repair costs of the proposed system were calculated based on the 20-year lifespan, which is a typical value for a chemical engineering facility (Park et al., 2025). The hydrogen gas produced in the cathodic chamber was assumed to be sold as revenue.

For the proposed system of a scaled-up plant, the overall CAPEX was 4.109 M$, while OPEX was estimated as 3.191 M$. The cost of the electrolyzer was 0.398 M$, estimated from the sixth-tenth rule. Assuming that a commercial PEM electrolyzer is employed, the CAPEX would be reduced because of the cheaper prices of commercial products than customized products. If the electrolyzer is replaced with a 10 PEM electrolyzer, in which the same current is applied, the purchase cost is reduced from 0.398 to 0.155 M$; consequently, the CAPEX decreases to 2.524 M$. Along with the electrolyzer cost, the adsorption tower and CAPEX costs could be reduced. OPEX reduction costs can be accomplished through the improvement of the electrolyzer efficiency. For instance, the electricity cost is 2.201 M$, which accounts for ~69 % of the OPEX. If the operating voltage of 7 V decreases to 5 V, the OPEX can be improved to 2.555 M$.

The annual amount of hydrogen gas produced as a by-product was 98,000 kg. The revenue from the sale of hydrogen accounts for 0.669 M$

Table 3
Cost analysis of the proposed system.

Contents	Elements	Cost (M$)
CAPEX	Electrolyzer	0.398
	Adsorption tower	0.232
	Fixed capital investment	2.550
	Working capital	0.450
	Total capital investment	4.109
OPEX	Electricity	2.201
	Labor	0.065
	Water	0.001
	$NaNO_3$	0.350
	NaOH	0.073
	Adsorbent	0.037
	Total product cost	3.191
Revenue	Hydrogen gas sale	0.669

by considering a price of 6.83 $/kg. This amount is equivalent to an OPEX of 21 %; thus, the net OPEX is estimated to be 2.522 M$. However, neither CAPEX nor OPEX considered the equipment needed for the sale of the hydrogen gas—such as compressors, liquefaction devices, and storage—demonstrating an overcalculation. Nevertheless, CAPEX and OPEX must be reduced to less than the values in Table 3 owing to the benefits of hydrogen production.

To examine cost superiority, the CAPEX and OPEX were normalized to the system capacity (m^3/d) (Table 4). According to the normalized CAPEX and OPEX, the overall cost of the proposed system is possibly competitive, though more expensive than some technology, as compared with other advanced oxidation processes. Among the technologies listed in Table 4, Biological CSTR (continuous stirred-tank reactor), BNR (biological nutrient removal), ASP (activated sludge process), and AnMBR (Anaerobic sludge blanket and membrane reactor (AnMBR), which are cheaper than our estimation, are wastewater treatment technologies based on microbial behavior. Biological technologies are less expensive than physicochemical treatments (Mousset et al., 2021). Notably, the SBR (sequencing batch reactor) used by Ochs et al. (2023) reported a higher CAPEX of 4.703 K$/$m^3$/d than that of this study, despite the biotic process. This resulted from the difficulty of the biological treatment of the AD dewatering liquor. The liquor has non-biodegradable organics and a high TAN loading. Therefore, a large reactor volume and high organic chemical doses are required due to a prolonged reaction time, resulting in an increase in CAPEX and OPEX. This is consistent with the report by Ochs's group (Ochs et al., 2023). Ochs et al. additionally emphasized that biological TAN removal can emit N_2O gas, which is one of the greenhouse gases. This demonstrates that the biological treatment of TAN in the AD dewatering liquor is an inefficient approach.

The normalized cost of the proposed system is comparable to those of stripping, membranes, and ion exchange, which are advanced treatment technologies. Remarkably, ion exchange by Huang et al. and hydrogen gas production by Grasham et al. from AD wastewater were 16.150 and 25.439 M$, respectively. The cost was more than 4–6 times larger value than that found in this study. Huang and Grasham's research aim to obtain products from TAN in wastewater, unlike biological technology (Huang et al., 2020; Grasham et al., 2020). Consequently, additional equipment installation costs were incurred; however, the proposed system has a low cost, indicating its price superiority for resource recovery technology from wastewater. In summary, the proposed process provides an environmentally friendly and effective method for the abatement of TAN in AD dewatering liquor. Most importantly, this study verifies the stability and economic feasibility through a repeated-use test and cost estimation. Nevertheless, it is imperative to conduct pilot-scale and long-term experiments to obtain the optimized operating parameters and further assess the feasibility of practical applications.

Table 4
Normalized CAPEX and OPEX per system capacity of TAN removal technologies reported in the literatures.

System	Wastewater (C_{TAN})	System capacity	Cost (K$/$m^3$/d)		Ref.
			CAPEX	OPEX	
Biological CSTR	AD dewatering liquor (1700 mg-N/L)	1000 m^3/d	3.316[a]	0.380[a]	Ochs et al. (2023)
SBR			4.703[a]	1.414[a]	
Thermal stripping			4.210[a]	3.776[a]	
BNR	Wastewater influent (14 mg-N/L)	5400 m^3/d	0.943[a]	1.053[a]	Huang et al. (2020)
ASP + IX			0.833[a]	1.077[a]	
AnMBR + IX			0.861[a]	0.718[a]	
Ion exchange (N, P removal)	AD effluent (2917 mg-N/L)	120 m^3/d	16.150[a]	15.075[a]	
Stripping + Absorption + Reforming H_2	AD dewatering liquor (1500 mg-N/L)	661 m^3/d	25.439[a]	29.375[a]	Grasham et al. (2020)
Membrane	AD effluent (720 mg-N/L)	15 m^3/d	9.800[b]	3.533[b]	Rivera et al., 2023
Membrane Contactor	Reject water (1036 mg-N/L)	2500 m^3/d	3.333[b]	2.050[b]	Kaljunen et al., 2021
Ion exchange + Electrolysis	AD dewatering liquor (1000 mg-N/L)	1000 m^3/d	4.109	3.191	This study

[a] convert GBP to USD (rate:1.29 USD/GBP),
[b] convert EURO to USD (rate:1.08 USD/EUR).

4. Conclusions

A coupled system comprising ion exchange and electro-oxidation was proposed and tested for effective TAN removal and hydrogen gas production. To evaluate the practical applicability of the system, adsorption, desorption, and electro-oxidation processes were repeated for 12 cycles under realistic conditions. In addition to a series of experiments, the overall cost (CAPEX and OPEX) was estimated to determine economic feasibility. According to the experimental results, the proposed system showed stable TAN removal efficacy and a large capacity for PBA. Furthermore, the TAN recovered through PBA was effectively removed in the BPM-integrated electrolyzer without any changes in the TAN oxidation rate. Although the accumulation of nitrate in the regenerant was observed as a result of the oxidation of TAN to nitrate, it was negligible over 12 cycles, demonstrating short-term stability. In addition, the CAPEX and OPEX were comparable with those of other advanced oxidation processes reported in the literature for the treatment of dewatering liquor. In conclusion, the findings demonstrate that the proposed system enables TAN to recover and generate hydrogen gas, which is a waste-to-energy process. Finally, further research, including pilot- and full-scale studies, are required to obtain reliable operational data and results to fully realize the potential of the system.

CRediT authorship contribution statement

Jeong-Hee Kang: Writing – original draft, Validation, Resources, Investigation, Data curation. **Gyung-Geun Oh:** Validation, Resources, Data curation. **MyungSuk Son:** Writing – review & editing, Data curation. **Sungwon Kang:** Writing – review & editing, Supervision, Project administration, Conceptualization.

Funding

The authors greatly acknowledge and express their gratitude to the researchers supporting grant number (Grant number: 20250242-001), Korea Institute of Civil Engineering and Building Technology (KICT).

Declaration of competing interest

The authors declare that they have no known competing financial interests or personal relationships that could have appeared to influence the work reported in this paper.

Appendix A. Supplementary data

Supplementary data to this article can be found online at https://doi.org/10.1016/j.jenvman.2025.126661.

Data availability

Data will be made available on request.

References

Ahn, S.K., Park, K.Y., Song, W.J., Park, Y.M., Kweon, J.H., 2022. Adsorption mechanisms on perfluorooctanoic acid by FeCl3 modified granular activated carbon in aqueous solutions. Chemosphere 303, 134965. https://doi.org/10.1016/j.chemosphere.2022.134965.

Bunce, N.J., Bejan, D., 2011. Mechanism of electrochemical oxidation of ammonia. Electrochim. Acta 56 (24), 8085–8093. https://doi.org/10.1016/j.electacta.2011.07.078.

Cho, K., Hoffmann, M.R., 2017. Molecular hydrogen production from wastewater electrolysis cell with multi-junction BiOx/TiO2 anode and stainless steel cathode: current and energy efficiency. Appl. Catal. B Environ. 202, 671–682. https://doi.org/10.1016/j.apcatb.2016.09.067.

Dai, Z., Yu, Y., Hao, W., Chen, C., Ao, M., Yao, J., Yang, C., Liang, H., Guo, C., Han, L., 2024. Alkali-driven Donnan dialysis for efficient ammonia recovery from wastewater: performance, mechanism and optimization. Chem. Eng. J. 496, 154129. https://doi.org/10.1016/j.cej.2024.154129.

Fan, S., Wang, Y., Li, Y., Tang, J., Wang, Z., Tang, J., Li, X., Hu, K., 2017. Facile synthesis of tea waste/Fe 3 O 4 nanoparticle composite for hexavalent chromium removal from aqueous solution. RSC Adv. 7 (13), 7576–7590. https://doi.org/10.1039/C6RA27781K.

Gendel, Y., Lahav, O., 2013. A novel approach for ammonia removal from fresh-water recirculated aquaculture systems, comprising ion exchange and electrochemical regeneration. Aquac. Eng. 52, 27–38. https://doi.org/10.1016/j.aquaeng.2012.07.005.

Grasham, O., Dupont, V., Cockerill, T., Camargo-Valero, M.A., Twigg, M.V., 2020. Hydrogen via reforming aqueous ammonia and biomethane co-products of wastewater treatment: environmental and economic sustainability. Sustain. Energy Fuels 4 (11), 5835–5850. https://doi.org/10.1039/D0SE01335H.

Han, J.H., Jwa, E., Lee, H., Kim, E.J., Nam, J.Y., Hwang, K.S., Jeong, N., Choi, J., Kim, H., Jeung, Y., Chung, T.D., 2022. Direct seawater electrolysis via synergistic acidification by inorganic precipitation and proton flux from bipolar membrane. Chem. Eng. J. 429, 132383. https://doi.org/10.1016/j.cej.2021.132383.

Huang, X., Guida, S., Jefferson, B., Soares, A., 2020. Economic evaluation of ion-exchange processes for nutrient removal and recovery from municipal wastewater. npj Clean Water 3 (1), 7. https://doi.org/10.1038/s41545-020-0054-x.

Inyinbor, A.A., Adekola, F.A., Olatunji, G.A., 2016. Kinetics, isotherms and thermodynamic modeling of liquid phase adsorption of Rhodamine B dye onto Raphia hookerie fruit epicarp. Water Resour. Ind. 15, 14–27. https://doi.org/10.1016/j.wri.2016.06.001.

Im, S., Lee, H., Kim, T., Jeon, H., Jang, A., 2025. Application of non-acid stripping solution in hydrophobic membrane process for high-purity ammonia recovery from high-strength ammonium wastewater. Sep. Purif. Technol. 357, 129998. https://doi.org/10.1016/j.seppur.2024.129998.

Kang, J.H., Oh, G.G., Lee, B.J., Im, S., Kim, W., Kang, S., Han, J.H., 2024. Direct electrooxidation of ammonia-enriched wastewater using a bipolar membrane-integrated electrolytic cell. Water 16 (11), 1599. https://doi.org/10.3390/w16111599.

Kang, S., Lee, B., Ahn, K.H., Im, S., Kim, B., Kim, T.H., Hwang, Y., Chae, S., 2023. Facile synthesis of copper-substituted Prussian blue analog immobilized ion exchange resins for high-performance ammonium recovery from wastewater: adsorption kinetics, isotherms, and regeneration. Chem. Eng. J. 457, 141128. https://doi.org/10.1016/j.cej.2022.141128.

Krishnan, S., Koning, V., de Groot, M.T., de Groot, A., Mendoza, P.G., Junginger, M., Kramer, G.J., 2023. Present and future cost of alkaline and PEM electrolyser stacks. Int. J. Hydrogen Energy 48 (83), 32313–32330. https://doi.org/10.1016/j.ijhydene.2023.05.031.

Kuang, W., Yan, Z., Chen, J., Ling, X., Zheng, W., Huang, W., Feng, C., 2022. A bipolar membrane-integrated electrochlorination process for highly efficient ammonium removal in mature landfill leachate: the importance of ClO• generation. Environ. Sci. Technol. 57 (47), 18538–18549. https://doi.org/10.1021/acs.est.2c05735.

Lahav, O., Schwartz, Y., Nativ, P., Gendel, Y., 2013. Sustainable removal of ammonia from anaerobic-lagoon swine waste effluents using an electrochemically-regenerated ion exchange process. Chem. Eng. J. 218, 214–222. https://doi.org/10.1016/j.cej.2012.12.043.

Largitte, L., Pasquier, R., 2016. A review of the kinetics adsorption models and their application to the adsorption of lead by an activated carbon. Chem. Eng. Res. Des. 109, 495–504. https://doi.org/10.1016/j.cherd.2016.02.006.

Lee, B., Chae, H., Choi, N.H., Moon, C., Moon, S., Lim, H., 2017. Economic evaluation with sensitivity and profitability analysis for hydrogen production from water electrolysis in Korea. Int. J. Hydrogen Energy 42 (10), 6462–6471. https://doi.org/10.1016/j.ijhydene.2016.12.153.

Li, G., Wang, T., Xue, Y., Li, H., Liu, D., 2025. Construction of low-vacancy hexagonal Prussian blue analogues for efficient rubidium recovery. Sep. Purif. Technol. 359, 130842. https://doi.org/10.1016/j.seppur.2024.130842.

Li, M., Feng, C., Zhang, Z., Zhao, R., Lei, X., Chen, R., Sugiura, N., 2009. Application of an electrochemical-ion exchange reactor for ammonia removal. Electrochim. Acta 55 (1), 159–164. https://doi.org/10.1016/j.electacta.2009.08.027.

Liu, H., Yang, C.J., Dong, C.L., Wang, J., Zhang, X., Lyalin, A., Taketsugu, T., Chen, Z., Guan, D., Xu, X., Shao, Z., Huang, Z., 2024. Electrocatalytic ammonia oxidation to nitrite and nitrate with NiOOH-Ni. Adv. Energy Mater. 14 (42), 2401675. https://doi.org/10.1002/aenm.202401675.

Liu, X., Elgowainy, A., Wang, M., 2020. Life cycle energy use and greenhouse gas emissions of ammonia production from renewable resources and industrial by-products. Green Chem. 22 (17), 5751–5761. https://doi.org/10.1039/D0GC02301A.

Lizarralde, I., Guida, S., Canellas, J., Jefferson, B., Grau, P., Soares, A., 2021. Development and calibration of a new mathematical model for the description of an ion-exchange process for ammonia removal in the presence of competing ions. Water Res. 206, 117779. https://doi.org/10.1016/j.watres.2021.117779.

Ma, D., Zou, X., Li, R., Chen, P., Wang, Y., Chen, T., Zhang, Q., Liu, H., Chen, Y., Lv, W., Feng, Y., Liu, G., 2020. Highly efficient adsorption of Pb (II) by cubic nanocrystals in aqueous solution: behavior and mechanism. Arab. J. Chem. 13 (5), 5229–5240. https://doi.org/10.1016/j.arabjc.2020.02.022.

Mousset, E., Loh, W.H., Lim, W.S., Jarry, L., Wang, Z., Lefebvre, O., 2021. Cost comparison of advanced oxidation processes for wastewater treatment using accumulated oxygen-equivalent criteria. Water Res. 200, 117234. https://doi.org/10.1016/j.watres.2021.117234.

Nativ, P., Ben-Asher, R., Fridman-Bishop, N., Lahav, O., 2021. Synthesis and characterization of zinc-hexacyanoferrate composite beads for controlling the ammonia concentration in low-temperature live seafood transports. Water Res. 203, 117551. https://doi.org/10.1016/j.watres.2021.117551.

Nativ, P., Derbew, Z.A., Dagan-Jaldety, C., Aviezer, Y., Ben-Asher, R., Lahav, O., 2022. Sustainable removal of ammonia from the anaerobic digester supernatant line using a Prussian blue analogue (PBA) composite adsorbent. ChemEngineering 6 (6), 97. https://doi.org/10.3390/chemengineering6060097.

Nguyen, T.D., Nguyen, T.M.P., Van, H.T., Nguyen, L.H., Nguyen, T.D., Nguyen, T.H.V., Chu, T.H.H., Nguyen, T.H., Ha, L.T., Vinh, N.D., Thai, V.N., Nguyen, V.Q., Nguyen, K.A., Thang, P.Q., 2022. Adsorption removal of ammonium from aqueous solution using Mg/Al layered double hydroxides-zeolite composite. Environ. Technol. Innovat. 25, 102244. https://doi.org/10.1016/j.eti.2021.102244.

Ochs, P., Martin, B., Germain-Cripps, E., Stephenson, T., van Loosdrecht, M., Soares, A., 2023. Techno-economic analysis of sidestream ammonia removal technologies: biological options versus thermal stripping. Environ. Sci. Ecotechnol. 13, 100220. https://doi.org/10.1016/j.ese.2022.100220.

Parajuli, D., Noguchi, H., Takahashi, A., Tanaka, H., Kawamoto, T., 2016. Prospective application of copper hexacyanoferrate for capturing dissolved ammonia. Ind. Eng. Chem. Res. 55 (23), 6708–6715. https://doi.org/10.1021/acs.iecr.6b00748.

Park, J., Kang, S., Kim, S., Kim, H., Cho, H.S., Lee, J.H., 2025. Comparative techno-economic evaluation of alkaline and proton exchange membrane electrolysis for hydrogen production amidst renewable energy source volatility. Energy Convers. Manag. 325, 119423. https://doi.org/10.1016/j.enconman.2024.119423.

Sumalinog, D.A.G., Capareda, S.C., de Luna, M.D.G., 2018. Evaluation of the effectiveness and mechanisms of acetaminophen and methylene blue dye adsorption on activated biochar derived from municipal solid wastes. J. Environ. Manag. 210, 255–262. https://doi.org/10.1016/j.jenvman.2018.01.010.

Thommes, M., Kaneko, K., Neimark, A.V., Olivier, J.P., Rodriguez-Reinoso, F., Rouquerol, J., Sing, K.S., 2015. Physisorption of gases, with special reference to the evaluation of surface area and pore size distribution (IUPAC technical report). Pure Appl. Chem. 87 (9–10), 1051–1069. https://doi.org/10.1515/pac-2014-1117.

Tian, X., Gao, Z., Feng, H., Zhang, Z., Li, J., Wang, A., 2019. Efficient nutrient recovery/removal from real source-separated urine by coupling vacuum thermal stripping with activated sludge processes. J. Clean. Prod. 220, 965–973. https://doi.org/10.1016/j.jclepro.2019.02.181.

Usuda, H., Mishima, Y., Kawamoto, T., Minami, K., 2022. Desorption of ammonia adsorbed on prussian blue analogs by washing with saturated ammonium hydrogen carbonate solution. Molecules 27 (24), 8840. https://doi.org/10.3390/molecules27248840.

U.S. Geological Survey, 2024. Mineral Commodity Summaries 2024. U.S. Geological Survey. https://doi.org/10.3133/mcs2024.

Vigneswaran, V.S., Gowd, S.C., Ravichandran, V., Karthikeyan, M., Ganeshan, P., Kandasamy, S., Lee, J., Barathi, S., Rajendran, K., 2025. Green ammonia as hydrogen carrier: current status, barriers, and strategies to achieve sustainable development goals. Sci. Total Environ. 982, 179646. https://doi.org/10.1016/j.scitotenv.2025.179646.

Wang, Y., Meyer, T.J., 2019. A route to renewable energy triggered by the Haber-Bosch process. Chem 5 (3), 496–497. https://doi.org/10.1016/j.chempr.2019.02.021.

Wan, Z., Tao, Y., Shao, J., Zhang, Y., You, H., 2021. Ammonia as an effective hydrogen carrier and a clean fuel for solid oxide fuel cells. Energy Convers. Manag. 228, 113729. https://doi.org/10.1016/j.enconman.2020.113729.

Wu, F.C., Tseng, R.L., Juang, R.S., 2009. Characteristics of Elovich equation used for the analysis of adsorption kinetics in dye-chitosan systems. Chem. Eng. J. 150 (2–3), 366–373. https://doi.org/10.1016/j.cej.2009.01.014.

Zhang, Z., Zhao, L., Chen, J., Wang, Y., Liu, Y., Hou, X., Qu, J., Lv, C., Hu, Q., 2025. Ultra-strong adsorption of ammonia nitrogen from low-temperature and complex systems by Prussian blue analogue. Sep. Purif. Technol. 355, 129700. https://doi.org/10.1016/j.seppur.2024.129700.

Zhao, Q.B., Ma, J., Zeb, I., Yu, L., Chen, S., Zheng, Y.M., Frear, C., 2015. Ammonia recovery from anaerobic digester effluent through direct aeration. Chem. Eng. J. 279, 31–37. https://doi.org/10.1016/j.cej.2015.04.113.